Radiative electron capture by high-energy oxygen ions in hydrogen and helium

C. R. Vane, S. Datz, P. F. Dittner, J. Giese,* N. L. Jones, H. F. Krause, and T. M. Rosseel
Oak Ridge National Laboratory, P.O. Box 2008, Oak Ridge, Tennessee 37831-6377

R. S. Peterson
Department of Physics, University of the South, Sewanee, Tennessee 37375
(Received 4 October 1993)

X rays produced in the collisions of 94–222-MeV O^{8+} ions with H_2 and He targets have been measured. Resulting spectra have been analyzed to determine absolute yields, profile widths, and energies for x rays emitted in the process of radiative electron capture (REC). These measurements are compared with predictions based on impulse-approximation calculations, using differential cross sections for radiative recombination (RR) folded with target Compton profiles. Measured absolute peak energy positions and profiles are found to be in good agreement with these simple theoretical estimates. Cross sections derived from REC yields are compared with other measurements and with theoretical RR values. A small systematic discrepancy between experimental and theoretical cross sections is noted.

PACS number(s): 34.70.+e

I. INTRODUCTION

X-ray spectra observed in fast heavy-ion collisions consist of discrete energy, characteristic projectile, and target x-ray lines superimposed on a continuum background arising mainly from primary- and secondary-electron bremsstrahlung. In addition to these features, broad peaks appear in the spectra which originate from photons emitted during direct transfer of slow target (B) electrons to bound states of the moving projectile ion (A) in the reaction

$$A^{q+}+B\rightarrow A^{(q-1)+}(n)+B^{+}+\hbar\omega(n_{\mathrm{REC}}) .$$

This last process has been called radiative electron capture (REC) and is further categorized by explicitly identifying the final-state atomic shell (n_{REC}); e.g., K REC corresponds to x rays emitted in transfer of electrons to the ion's K shell, L REC transfer to the L shell, etc.

Radiative electron capture is closely related to the fundamental neutralization process of radiative recombination (RR) [1], in which a free electron is transferred into a bound state of a positive ion, with simultaneous emission of a momentum- and energy-conserving photon acting as the necessary third body. Radiative recombination is the exact inverse of the photoelectric effect. REC is distinguished from RR in that the active electron in REC initially occupies a bound state in the target.

K REC was first observed by Schnopper *et al.* [2] in 1972. Since then, many experimental studies of REC have been reported for a wide variety of conditions, in gas and solid targets [3–10]. Substantial theoretical interest has also resulted [11–14]. There remain, however, several unsettled discrepancies between experiments and theory. In particular, precise absolute measurements of K REC peak positions for bare ions channeled through thin single crystals have exhibited small shifts toward lower energy than predicted by simple energy-conservation considerations [15]. Measured cross sections for heavy ions in H_2 and He gas targets have also tended to lie 20–30% lower than expected [16]. Our motivation for the work reported here was to test whether or not these discrepancies remained in REC data from gas targets and for previously unexplored regions of ion charge and energy.

The REC process is most easily described in the rest frame of the moving ions. In that frame, the energy of each REC photon is given (nonrelativistically) by energy conservation as

$$\hbar\omega_{\mathrm{REC}}=E_p^{\mathrm{BE}}+(E_{\mathrm{rel}}^{\mathrm{KE}}+E_{\mathrm{T}}^{\mathrm{PE}}) , \tag{1}$$

where E_p^{BE} is the binding energy of the active electron in the projectile final state and $(E_{\mathrm{rel}}^{\mathrm{KE}}+E_T^{\mathrm{PE}})$ is the electron's initial total energy, relative to the projectile. The relative energy for a given (unperturbed) target electron momentum $\mathbf{p}_{\mathrm{T}}$ is (nonrelativistically)

$$(E_{\mathrm{rel}}^{\mathrm{KE}}+E_{\mathrm{T}}^{\mathrm{PE}})=\tfrac{1}{2}m_e v_p^2+\mathbf{v}_p\cdot\mathbf{p}_{\mathrm{T}}-E_{\mathrm{T}}^{\mathrm{BE}} , \tag{2}$$

where m_e is the electron mass, v_p is the projectile velocity, and $E_{\mathrm{T}}^{\mathrm{BE}}$ is the positive binding energy of the electron in its initial state.

When the ion's velocity is significantly greater than the average orbital speed of the target electron, the impulse approximation is often applied [17]. Weakly bound electrons are then treated as quasifree, with relative kinetic energies E_{rel} distributed about $\frac{1}{2}m_e v_p^2$, according to the probability profile of the initial target electron momentum distribution. The REC energy, at the peak of the distribution, is then given by

$$\hbar\omega_{\mathrm{REC}}=E_p^{\mathrm{BE}}+E_0-E_{\mathrm{T}}^{\mathrm{BE}} , \tag{3}$$

where $E_0=\frac{1}{2}m_e v_p^2$. Within this approximation, K REC

*Present address: Department of Physics and Astronomy, Kansas State University, Manhattan, KS 66506.

by a bare ion from a target with electron momentum wave function $\Psi_T(\mathbf{p}_T)$ may be expressed in terms of the RR cross section $[d\sigma_{RR}/d\Omega]$ at laboratory angle θ_L given by Bethe and Salpeter [1] as

$$\frac{d^2\sigma_{REC}}{d\Omega d\hbar\omega}=\int d^3p\,|\Psi_T(\mathbf{p}_T)|^2\left[\frac{d\sigma_{RR}}{d\Omega}\right]_{E_{rel}}\times\delta(\hbar\omega_{REC}-E_{rel}-E_p^{BE}+E_T^{BE}),$$
$$\left[\frac{d\sigma_{RR}}{d\Omega}\right]_{E_{rel}}=1.09\times10^{-21}\left[\frac{cm^2}{sr}\right]F(\kappa)\times\sin^2\theta_2/(1-\beta\cos\theta_L)^4,$$
$$F(\kappa)=\left[\frac{\kappa^3}{1+\kappa^2}\right]^2\frac{\exp\{-4\kappa\tan^{-1}(1/\kappa)\}}{[1-\exp(-2\pi\kappa)]},\qquad(4)$$
$$\kappa=\left[\frac{E_p^{BE}}{E_{rel}^{KE}}\right]^{1/2},$$

and $\beta=v_p/c$ (c is the velocity of light). The K REC peak observed in ion-induced x-ray spectra then corresponds, within this model, to a fold of the RR process with the momentum distribution of the electrons being captured. The δ function in Eq. (4) ensures energy conservation as specified in Eqs. (1) and (2). For narrow target distributions, where "narrow" means that $[d\sigma_{RR}/d\Omega]$ varies little over the relevant momentum width, $[d\sigma_{RR}/d\Omega]$ may be replaced with its central value at E_0 and removed from the integral:

$$\frac{d^2\sigma_{REC}}{d\Omega d\hbar\omega}=\left[\frac{d\sigma_{RR}}{d\Omega}\right]_{E_0}\int d^3p\,|\Psi_T(\mathbf{p}_T)|^2\times\delta(\hbar\omega_{REC}-E_{rel}-E_p^{BE}+E_T^{BE}).\qquad(5)$$

The remaining integral is just the target Compton profile [18], divided by v_p. The shape of the K REC peak should therefore mimic the Compton profile for a given target, with some minor distortion due to variation of the capture probability over the profile width. The peak energy is given in Eq. (3), since the Compton profile normally maximizes sharply at $\mathbf{v}_p\cdot\mathbf{p}_T=0$.

In the laboratory frame, x rays emitted from the projectile are energy shifted according to the relativistic Doppler equation as

$$\hbar\omega_{lab}=\hbar\omega/\gamma(1-\beta\cos\theta_L),\qquad(6)$$

where $\gamma=(1-\beta^2)^{-1/2}$. The REC peak is shifted in energy and slightly distorted by this effect. The observed REC peak is also shifted and distorted by effects of the underlying continuum x rays, which arise from two main bremsstrahlung contributions. Up to a photon energy of $\sim\frac{1}{2}m_ev_p^2$, the dominant source of background is from bremsstrahlung radiation produced in direct Coulomb scattering of target electrons from the massive projectile ions. This process is termed primary bremsstrahlung (PB) and extends up to an endpoint energy given by the relative energy of the target electrons measured with respect to the ion. Alternatively, PB may be viewed as radiative capture into continuum states of the projectile. The PB spectrum has been calculated in the plane-wave Born approximation by Heitler [19] and is treated by Bethe and Salpeter [1], and has the form

$$\left[\frac{d^2\sigma_{PB}}{d\Omega d\hbar\omega}\right]_{\theta_L=90^\circ}=6.28\times10^{-23}\ (cm^2/eV\,sr)\times\frac{Z_p^2}{E_{rel}\hbar\omega_{PB}}\times\ln\left[\frac{\sqrt{E_{rel}}+\sqrt{E_{rel}-\hbar\omega}}{\sqrt{E_{rel}}-\sqrt{E_{rel}+\hbar\omega}}\right]\times\frac{21E_{rel}}{(22E_{rel}-8\hbar\omega_{PB})},\qquad(7)$$

where E_{rel} and $\hbar\omega_{PB}$ are given in units of eV. The last term in Eq. (7) is a linear approximation polarization factor. Like REC, the shape of the PB spectrum near its end point reflects the momentum distribution of the target electrons.

Significantly above $\sim\frac{1}{2}m_ev_p^2$, another process, called secondary electron bremsstrahlung (SEB), dominates. In SEB target electrons scattered up to energies $\sim4(\frac{1}{2}m_ev_p^2)$ may subsequently radiatively rescatter from target atoms or from atoms in the walls of the gas cell. From previous measurements and calculations [19], SEB intensities are expected to be weak for H_2 and He targets and to decrease slowly and smoothly with photon energy. SEB backgrounds then have little effect on REC peak shapes and positions, while PB intensities, which vary rapidly near the low-energy wing of the REC peak for light ions, have significantly greater effect.

The relative and absolute yields of PB, SEB, and REC x rays depend strongly on the angle of observation. For nonrelativistic energies $\beta\ll1$, $d\sigma_{RR}/d\Omega$ from Eq. (4) varies as $\sim\sin^2\theta_L$. PB yields have a similar angular distribution, while SEB x rays are expected to be distributed nearly uniformly [19]. Accurate measurements of REC yields require proper accounting for the PB and SEB backgrounds.

In this work, we report measurements made of K REC x rays produced in collisions of 100–225-MeV O^{8+} ions with H_2 and He in a closed target cell. Centroid energies of the REC peaks observed are compared with theory incorporating corrections for a number of substantial energy shifting mechanisms. The K-shell binding energy for O^{7+} ($1s$) is extracted from these corrected peak energies and compared with calculations. Measured REC peak profile widths are compared with widths calculated using Hartree-Fock Compton profiles for H and He [20]. Finally, K REC cross sections are extracted from measured x-ray yields and compared with other recent high-energy measurements [16], and with estimates based on calculated RR cross sections. Except for a general unexplained 20–30 % lower than expected cross section, our measurements of REC energies, profile widths, and yields agree well with theory.

II. EXPERIMENTAL METHODS

Fully stripped 100–225-MeV O ions from the Holifield Heavy Ion Research Facility 25-MV Tandem accelerator located at Oak Ridge National Laboratory were passed through a closed cell containing H_2 and He target gases. X rays emitted were measured using a Si(Li) detector. Transmitted ions were collected in a biased Faraday cup and charge was accumulated, digitized, and converted to the total number of collected ions for normalization of detected x rays. A schematic of the apparatus is shown in Fig. 1.

Oxygen ions were accelerated, stripped of their electrons, and magnetically selected using a 90° analyzing magnet with an absolute energy resolution of $<0.1\%$ [21]. The resulting beams were collimated to less than 2-mrad divergence by a pair of 3-mm-diam apertures separated by 2 m, the last located 0.5 m upstream of the target cell. The ions were collected in a deep, secondary electron suppressed Faraday cup located 0.7 m downstream of the gas cell. Typical beam currents used were 5–20 nA.

Entrance and exit to the gas cell were sealed by rolled 0.2-mg/cm^2 aluminum foils. The foil thickness was determined by direct weighting and by conversion from measured energy loss of 5.8-MeV ^{244}Cm α particles through use of the tabulated stopping power [22]. Gas pressures were varied between 0 and 30 Torr and measured using a calibrated Wallace and Tiernan Bourdon gauge. Ion energy losses in the gas cell entrance window varied from 6.3 MeV at 100 MeV to 3.5 MeV at 225 MeV, as calculated using STOPX [23], a computer program which incorporates Ref. [22] stopping powers in numerical integration calculations of total energy loss. The calculated losses are expected to be accurate to better than $\pm 10\%$ [22]. Mean energy loss in the gas targets never exceeded 0.2 MeV.

Contamination of the bare O^{8+} beam by one-electron ions formed in the window and gas by electron capture was calculated at each energy using tabulated equilibrium charge state fractions from Wittkower and Betz [24]. The expected O^{8+} fraction at the center of the cell varied from 85% to 100 MeV to more than 98% at 225 MeV.

A slotted aluminum and lead x-ray collimator assembly located at right angles to the beam limited detection of x rays to those originating from the central 3.8 mm of ion-target gas interaction volume and to emission angles of $89.1 \pm 2.5°$. The source volume and range of included angles were measured using a laser beam aligned through the ion collimators and reflecting from a front surface mirror mounted on a translatable goniometer at the center of the gas cell. The solid angle accepted by the collimator and subtended by the detector was 3.75×10^{-3} sr.

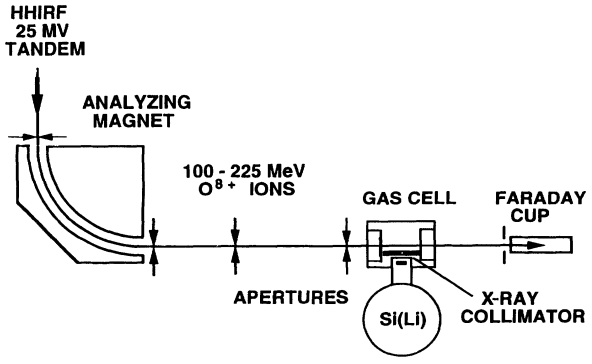

FIG. 1. Schematic of experimental apparatus.

X rays were detected in a liquid-nitrogen-cooled Si(Li) detector with an active detector area of 12.5 mm^2. signals were processed employing standard nuclear electronic techniques and stored using a multichannel analyzer. Energy calibration (to an accuracy of ± 5 eV) was performed using ^{55}Fe and ^{241}Am radioactive sources and Al K x rays from fluorescence by Mn x rays. Total ion induced x-ray count rates were maintained at less than 200/sec to avoid pulse pileup spectral distortion effects and to minimize acquisition dead time. Energy positions of background characteristic x rays from Al, Fe, Ni, and Pb, arising from scattered particles striking the stainless-steel walls of the target cell and the x-ray collimator were monitored during data acquisition to ensure stability of the energy calibration. The system energy resolution was measured to be 165 eV, full width at half maximum (FWHM), at 5.9 keV.

Low-energy x rays (e.g., oxygen K x rays) were absorbed in the Si(Li) detector entrance window (7.6-μm-thick Be) and in the detector 500-Å-thick front-surface gold contact and a 3000-Å-thick silicon dead layer. Correcting for these absorption effects using tabulated mass-absorption cross sections [25], the detection efficiency was calculated to vary from 25% for 1.0-keV x rays to $>98\%$ for 10.0-keV x rays. Peak energies of K REC x rays of interest here varied from ~ 4 to 8 keV, a region in which Si(Li) efficiency remains fairly constant and high (88–94%).

The number of K REC photons N_{REC}, detected in solid angle $\Delta\Omega(\theta_L)$ centered at angle θ_L for N_{ion} O^{8+} ions passing through a target atomic density ρ_T and length l_T is given by

$$N_{\mathrm{REC}} = n_K N_{\mathrm{ion}} \frac{d\sigma_{\mathrm{REC}}}{d\Omega} \Delta\Omega(\theta_L) \rho_T l_T n_e D_{\mathrm{eff}}(\hbar\omega_{\mathrm{REC}}) \ . \quad (8)$$

Here n_K is the number of K vacancies per ion, n_e is the number of target electrons in each target atom or molecule, and $D_{\mathrm{eff}}(\hbar\omega_{\mathrm{REC}})$ is the detection efficiency. Inverting Eq. (8), we derive the REC cross section at θ_L from the yield per ion $(N_{\mathrm{REC}}/N_{\mathrm{Ions}})$ and other measured quantities as

$$\frac{d\sigma_{\mathrm{REC}}}{d\Omega(\theta_L)} = \frac{N_{\mathrm{REC}}/N_{\mathrm{ions}}}{\Delta\Omega(\theta_L)\rho_T l_T n_e D_{\mathrm{eff}}(\hbar\omega_{\mathrm{REC}}) n_K} \ . \quad (9)$$

According to Eq. (4), the total K REC cross section is related to the differential cross section at 90° by

$$\sigma_{\mathrm{REC}} = \frac{8\pi}{3} \left[\frac{d\sigma_{\mathrm{REC}}}{d\Omega} \right]_{90°} \ . \quad (10)$$

III. RESULTS AND DISCUSSION

Typical x-ray spectra obtained for O^{8+} + H_2 are shown in Fig. 2 for ion energies at the gas cell center of 93.7, 135, 186, and 213 MeV. These data have been corrected for small backgrounds observed at zero gas pressure, generated by scattering of the ions from the Al gas cell window. The remaining Al K and Pb M lines appearing near 1.5 and 2.3–3.1 keV, respectively, arise mainly from recoiling target atoms which strike the Al and Pb collimator located directly in front of the Si(Li) detector. Oxygen K REC peaks for all four beam energies are also indicated in the figure. Measurements were made at several gas pressures from 0 to 30 Torr to establish linearity of x-ray yields. Similar spectra were obtained for He targets at energies of 93.7, 135, 186, 212, and 222 MeV.

Spectral data were first corrected for detector efficiency variation as a function of x-ray energy. The spectra were then least-squares fitted with Gaussian line shapes to account for the Al and Pb lines, with a continuum Pb theoretical component according to Eq. (7), and with an exponentially decreasing background chosen to simulate continuum SEB contributions. K REC peaks were simultaneously fitted, assuming peaks shapes given by asymmetric Gaussians with exponential tails. The K REC peak positions, low- and high-energy half widths at half maximum, and areas above background were output from the fits. We note that significant continua background appear to extend in the data, all the way up to the low energy tails of the REC peaks. This is at first surprising, as the major backgrounds, PB, should have end points lying E_p^{BE} below the K REC peaks (e.g., ~870 eV below the K REC peak). The dashed curve in Fig. 2 shows the PB spectrum expected from Eq. (7) for 93.7-MeV ions. SEB backgrounds are expected to be weak and smoothly varying and cannot account for the deficit in the regions just below the REC peaks.

As Andersson and Burgdörfer [26] have recently pointed out, contributions of REC to excited states (i.e., L REC, M REC, etc.) up to the continuum limit can account for a significant fraction of the total radiative capture. For energetic light ions, the projectile binding-energy contributions $E_p^{BE}(n)$ to n REC energies are relatively small and separations between x rays from capture to various n levels are unresolved because of larger intrinsic target Compton widths. X-ray contributions for all n REC therefore "pile up" in the region between the K REC peak and the expected PB shoulder.

As noted above, K REC shapes should mimic the target Compton profile, so that REC peaks from He are expected to be broader than for H_2. A direct comparison of measured spectra for 100-MeV incident ions (93.7 MeV at the gas cell center) is given in Fig. 3. Data shown there have been corrected for energy-dependent detector efficiency and for gas-out backgrounds. Results of a simulation of the H_2 spectrum are indicated by the solid curve. The calculated spectrum was generated by folding the H_2 Compton profile [20] with $d\sigma_{RR}/d\Omega$ from Eq. (4) and adding contributions for PB and SEB. Effects of n REC were included by adding $1/n^3$-intensity scaled REC profiles, shifted down in energy from the K REC peak according to $n^{-2}E_p^{BE}(1s)$. Figure 4 shows FWHM widths taken from fits to the measured K REC peak data as a function of ion energy, after corrections for broadening due to detector resolution and for minor Doppler broadening (e.g., <75 eV at 135 MeV) from the finite opening angle subtended by the detector and the extended source. The solid curves display widths extracted from similar fits of REC profiles calculated using Hartree-Fock Compton profiles for H_2 and He [20]. Unlike previous measurements by Tawara, Richard, and Kawatsura [6] for 15–40-MeV $F^{8+,9+}$ + He, we find excellent agreement with calculated values over this energy range. We note that widths obtained using simple $1s$ hydrogenic Compton profiles calculated using the He ionization energy (24.6 eV) lead to significantly narrower peak widths than those observed here.

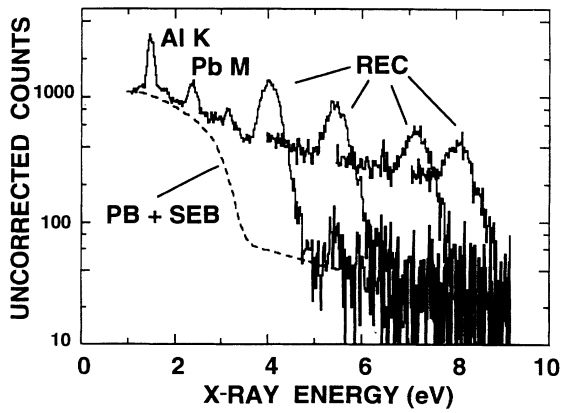

FIG. 2. X-ray spectra uncorrected for detector efficiency variations, for incident 100-, 140-, 190-, and 216-MeV O^{8+} ions and H_2 target gas. The background continuum of PB and SEB x rays calculated from Eq. (7) is displayed by the smooth curve for 100-MeV ions.

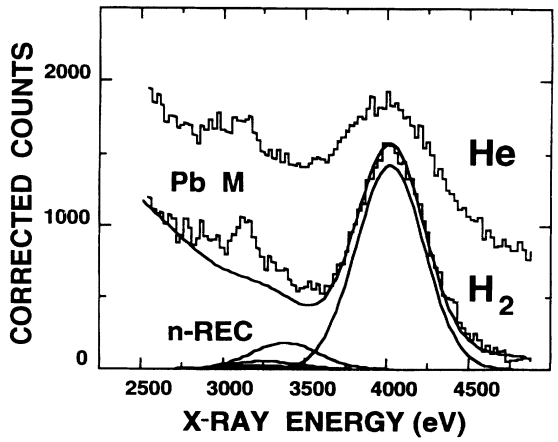

FIG. 3. X-ray spectra corrected for detector efficiency variation for incident 100-MeV O^{8+} ions and H_2 and He targets. The ion energy at the gas cell center is 93.7 MeV. The solid curve shows simulation results, with additional contributions from n REC included as indicated in the text.

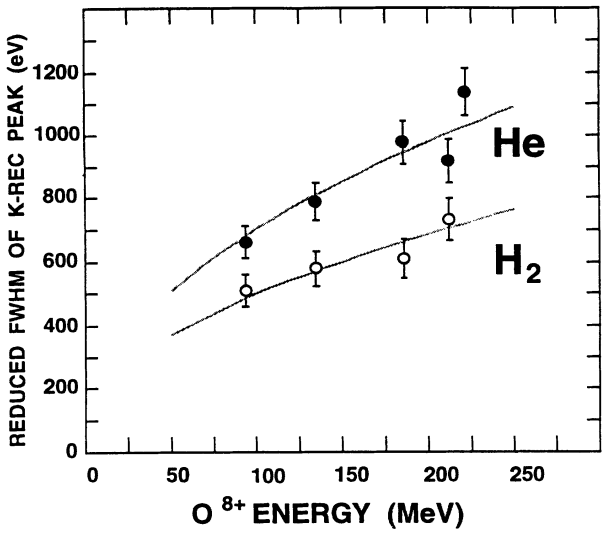

FIG. 4. Measured FWHM widths of K REC peaks for H_2 and He targets corrected for finite detector resolution broadening. Smooth curves display results of widths calculated from Hartree-Fock Compton profiles.

The REC peak-energy position varies nearly linearly with ion energy as expected from Eq. (3). However, the precise absolute peak energy observed is shifted from the simple value one might expect by a number of different mechanisms, most of which lead to a reduction in the measured value. We have calculated the magnitudes for each of these effects at each beam energy for both targets and tabulate the results in Tables I and II. The individual shifts are described below for 135-MeV O^{8+} + H_2.

The most important REC peak shift and uncertainty occurs because of ion energy loss in the gas cell entrance window. At an incident ion energy E_p of 140 MeV and 30 Torr gas pressure, the ion energy loss at the center of the cell is calculated to be 5.1±0.7 MeV. This results in a decrease of 176±24 eV in the mean relative energy of electrons as viewed by the ion, and, therefore in the energy of each REC photon. The next most significant effect is the relativistic Doppler shift. At a mean observation angle of 89.1°, REC x rays emitted from 135-MeV projectiles are shifted downward in the laboratory frame by −0.7%, or −37 eV. Variation of this shift over the observation opening angle is small. The third most important peak shifting mechanism is distortion arising from variation of the RR differential cross section across the target momentum distribution. We have estimated these shifts from results of fits to simulated spectra generated by convoluting the theoretical RR differential cross section [Eq. (2)] with Gaussian peaks having the measured REC profile widths at each energy. At 135 MeV, the RR variation shifts the REC peak position by −22 eV.

As noted previously, REC to excited states (n REC) produces x rays lying below the K REC peak energy. These x rays merge with the PB and SEB backgrounds in the low-energy tail of the K REC distribution creating an apparent shift and distortion in the K REC peak. We have investigated effects of REC to higher-n shells by determining shifts in fit results for K REC positions in the simulated spectra produced by adding a second set of broad Gaussian peaks, each shifted down in energy from the K REC peak according to $E_p^{\mathrm{BE}}(n)=871\ \mathrm{eV}/n^2$ and with relative areas scaled as $1/n^3$, as predicted for RR [1]. The K REC apparent shift due to n REC is small, −5 eV at 135 MeV, but increases with E_p because of increased broadening of the overlapping K REC and n REC components.

Contamination of the primary O^{8+} beam by hydrogenlike $O^{7+}(1s)$ formed in the gas and the cell entrance window leads to contaminate K REC x rays shifted from the bare ion peak by −132 eV, the difference in ionization energies of the $O^{8+}(1s)$ and $O^{7+}(1s^2)$. However, the fraction of O^{7+} ions at 100 MeV is small (<15%) and decreases with increasing ion energy. Also, the RR cross

TABLE I. Corrections to apparent $O^{8+}+H_2$ K REC peak energy position as described in the text. $E_p^{\mathrm{BEC}}(1s)$ is the $O^{7+}(1s)$ binding energy derived from the corrected measured REC peak energy $\hbar\omega_{\mathrm{REC}}^{\mathrm{corrected}}$ through Eq. (11). Unless indicated, energies are in units of eV.

E_p (MeV)	100	140	190	215
$\hbar\omega_{\mathrm{REC}}^{\mathrm{meas}}$	4024	5412	7134	8023
REC peak energy shifts				
E_p loss	−222	−176	−139	−125
Doppler	−18	−37	−70	−92
$d\sigma_{\mathrm{RR}}/d\hbar\omega$	−22	−22	−21	−18
n REC	−2	−5	−6	−12
O^{7+} contamination	−4	−4	−3	−3
D_{eff}	+3	+3	0	0
$\hbar\omega_{\mathrm{REC}}^{\mathrm{corrected}}$	4288	5652	7373	8267
$\hbar\omega_{\mathrm{REC}}^{\mathrm{calc}}$	4285	5651	7370	8262
$E_p^{\mathrm{BEC}}(1s)$	874	872	875	876

TABLE II. Corrections to apparent O^{8+}+He K REC peak energy position as described in the text. $E_p^{\mathrm{BEC}}(1s)$ is the $O^{7+}(1s)$ binding energy derived from the corrected measured REC peak energy $\hbar\omega_{\mathrm{REC}}^{\mathrm{corrected}}$ through Eq. (11). Unless indicated, energies are in units of eV.

E_p (MeV)	100	140	190	215	225
$\hbar\omega_{\mathrm{REC}}^{\mathrm{meas}}$	3987	5430	7104	7990	8283
REC peak energy shifts					
E_p loss	−222	−176	−139	−125	−122
Doppler	−18	−37	−70	−92	−99
$d\sigma_{\mathrm{RR}}/d\hbar\omega$	−40	−42	−44	−48	−42
n REC	−6	−13	−24	−24	−31
O^{7+} contamination	−9	−7	0	0	0
D_{eff}	+3	+3	0	0	0
$\hbar\omega_{\mathrm{REC}}^{\mathrm{corrected}}$	4278	5703	7381	8278	8577
$\hbar\omega_{\mathrm{REC}}^{\mathrm{calc}}$	4276	5642	7361	8253	8572
$E_p^{\mathrm{BEC}}(1s)$	873	932	891	896	876

section for single-K-vacancy ions is approximately half that for bare ions, so that the number of REC x rays from O^{7+} ions should be less than 7.5% of the O^{8+} yield. We have estimated the effects of a small portion of O^{7+} ions in the beam by applying our fitting procedures to spectra simulated by adding two identical profile peaks, with intensities given by expected RR cross sections and separated by 132 eV. At 135 MeV, the K REC peak position is found to shift by only -4 eV in response to an 8% component of one-electron ions.

The Si(Li) detection efficiency is relatively high and slowly varying in the region of interest, and the systematic change across the broad REC peaks causes only minor spectral distortions. These have been removed prior to fitting by dividing the raw data by efficiency as a function of x-ray energy. In tests of the impact of this procedure on peak position, we found that REC peaks would have been shifted by less than 0.2% (or 3 eV at 93.7 MeV) without this correction.

Having made all the above corrections to the measured REC peak positions at each ion energy, we compare, in Tables I and II, the corrected experimental values with calculations based on Eq. (1). Stöhlker *et al.* [16] have suggested using a similar method based on extrapolation of measured K REC peak energies to zero projectile velocity as a method for determining binding energies, especially for much heavier ions. We would like to point out that precise measurements using this method at high energies will require accurate evaluations of many of the shifting mechanisms that have been examined here, while measurements at low beam energies minimize some shifts (e.g., Doppler), but may enhance effects of others (e.g., $d\sigma_{RR}/d\Omega$ variation and charge-state contamination).

We have treated the projectile binding energy as unknown, and calculate it from the measurements by demanding equality of the corrected measured REC peak energy ($\hbar\omega_{REC}^{corrected}$) and the theoretical one, as

$$E_p^{BEC}(1s)=\hbar\omega_{REC}^{corrected}-\tfrac{1}{2}m_e v_p^2+E_T^{BE} . \quad (11)$$

The average of these values for H_2 and He at each energy is 885±30 eV, compared with the accepted Hartree-Fock calculated value of 871.4 eV [27]. The major components of the estimated error are due to uncertainties in projectile energy loss shifts and in errors in fitted peak positions from effects of background variations (both from PB plus SEB, and from REC to L and higher shells).

Areas of K REC peaks taken from fits of the efficiency corrected spectra have been converted to cross sections through Eq. (9) using n_K corrected for contaminate O^{7+} ion fractions. It has been noted by Stöhlker *et al.* [16] that K REC cross sections for gas targets over a wide range of projectiles and energies can be compared effectively when plotted against an "adiabaticity parameter" η, defined as the ratio of the central electron relative energy to the final-state binding energy of the active electron, as

$$\eta=\tfrac{1}{2}m_e v_p^2/E_p^{BE} . \quad (12)$$

In Fig 5, we display our measured K REC cross sections for bare O^{8+} ions along with other published REC measurements with H_2 and He targets as a function of η. RR

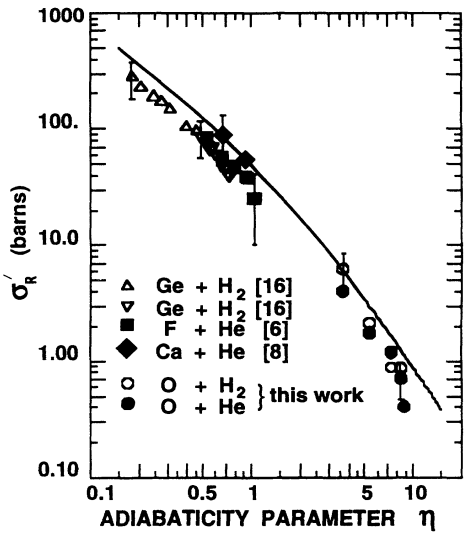

FIG. 5. Measured O^{8+} K REC cross sections per projectile K vacancy per target electron plotted versus adiabaticity parameter η as defined in the text, compared with Bethe-Salpeter results for radiative recombination. Other data are for H_2 and He targets and from references as indicated in the legend.

cross sections calculated from Eqs. (4) and (10) are also indicated by the smooth curve. Although most of the measurements lie within their individual estimated absolute errors from the RR curve, there is an obvious disagreement with theory for the data set taken as a whole. The bulk of the measurements lie consistently 20–30% lower than the Bethe-Salpeter RR results for η from 0.2 to 8.0. This discrepancy has been previously noted for gas targets by Stöhlker *et al.* [16] and by Tribedi *et al.* [28] for narrower ranges of η. Our data significantly expand the tested region and support their conclusions. We note that the data presented in Fig. 5 represent measurements for Z_p from 8 to 32 and for velocities from 5.6 to 23.6 a.u. The 20–30% discrepancy therefore appears to be a general feature of the process, independent of projectile charge and energy.

IV. CONCLUSION

We have measured REC x rays from energetic oxygen ions colliding with H_2 and He gases. The positions of K REC peaks agree well with calculated energies based on energy conservation, but only after correction for a number of significant shifting effects. The widths of the K REC peak profiles are well reproduced by estimations based on the impulse approximation using target Hartree-Fock Compton profiles. Areas of K REC peaks have been converted to cross sections which lie 20–30% below calculated K REC values based on cross sections for RR. Published K REC cross section data from several other measurements exhibit the same tendency.

ACKNOWLEDGMENTS

This research was sponsored by the U.S. Department of Energy, Office of Basic Energy Sciences, Division of Chemical Sciences, under Contract No. DE-AC05-84OR21400 with Martin Marietta Energy Systems, Inc.

[1] M. Stobbe, Ann. Phys. (Leipzig) **7**, 771 (1930); H. A. Bethe and E. E. Salpeter, *Quantum Mechanics of One- and Two-Electron Atoms* (Academic, New York, 1957), pp. 320–322.

[2] H. W. Schnopper, H. D. Betz, J. P. Delvaille, K. Kalata, and A. R. Shoval, Phys. Rev. Lett. **29**, 898 (1972).

[3] P. Kienle, M. Kleber, B. Povh, R. M. Diamond, F. S. Stephens, E. Grosse, M. R. Maiver, and D. Proetel, Phys. Rev. Lett. **31**, 1099 (1973).

[4] B. R. Appleton, R. H. Ritchie, J. A. Biggerstaf, T. S. Noggle, S. Datz, C. D. Moak, V. Verbeek, and V. N. Neelavathi, Phys. Rev. B **19**, 4347 (1979).

[5] T. Kambara, Y. Awaya, A. Hitachi, M. Kase, I. Kohno, and T. Tonuma, J. Phys. B **15**, 3759 (1982).

[6] H. Tawara, P. Richard, and K. Kawatsura, Phys. Rev. A **26**, 154 (1982).

[7] D. H. Jakubassa-Amundsen, R. Höppler, and H. D. Betz, J. Phys. B **17**, 3943 (1984).

[8] J. A. Tanis, M. W. Clark, K. H. Berkner, E. M. Bernstein, W. G. Graham, R. J. McDonald, R. H. McFarland, J. R. Mowat, D. W. Mueller, A. S. Schlachter, J. W. Stearns, and M. P. Stockli, J. Phys. (Paris) Colloq. **48**, C9-207 (1987); cross sections of Fig. 2 for Ca^{19+} and Ca^{20+} + He have been reduced by 20% to correct for a systematic error discovered after publication; J. A. Tanis (private communication).

[9] K. Kawatsura, A. Ootuka, M. Sataka, K. Komaki, H. Naramoto, K. Ozawa, Y. Nakai, and F. Fujimoto, Nucl. Instrum. Methods Phys. Res. Sect. A **262**, 33 (1987).

[10] S. Andriamonje, M. Chevalier, C. Cohen, J. Dural, M. J. Gaillard, R. Geure, M. Hage-Ali, R. Kirsch, A. L'Hoir, B. Mazuy, J. Mory, J. Moulin, J. C. Poizat, J. Remillieaux, D. Schmans, and M. Toulemoude, Phys. Rev. Lett. **59**, 2271 (1987).

[11] J. S. Briggs and K. Dettman, Phys. Rev. Lett. **33**, 1123 (1974); J. Phys. B **10**, 1113 (1977).

[12] R. Shakeshaft and L. Spruch, Phys. Rev. Lett. **38**, 175 (1977).

[13] M. Gorriz, J. S. Briggs, and S. Alton, J. Phys. B **16**, L665 (1983).

[14] J. E. Miraglia, Phys. Rev. A **32**, 2702 (1985); J. E. Miraglia, C. R. Garibotti, and A. D. Gonzalez, *ibid.* **32**, 250 (1985); M. C. Pacher, A. D. Gonzalez, and J. E. Miraglia *ibid.* **35**, 4108 (1987).

[15] C. R. Vane, P. F. Dittner, H. F. Krause, J. Gomez del Campo, N. L. Jons, P. A. Zeijlmans van Emmichoven, U. Bechthold, and S. Datz, Nucl. Instrum. Methods Phys. Res. Sect. B **67**, 256 (1992).

[16] Th. Stöhlker, C. Kozhuharov, A. E. Livingston, P. H. Mokler, Z. Stachura, and A. Warczak, Z. Phys. D **23**, 121 (1992); P. H. Mokler, Th. Stöhlker, C. Kozhuharov, Z. Stachura, and A. Warczak, *ibid.* **21**, 197 (1991); Th. Stöhlker, P. H. Mokler, C. Kozhuharov, E. A. Livingston, and J. Ullrich, Nucl. Instrum. Methods Phys. Res. Sect. B **56/57**, 86 (1991).

[17] M. Klebber and D. H. Jakubassa, Nucl. Phys. A **252**, 152 (1975).

[18] A. R. Shoval, J. P. Delvaille, K. Kalata, K. Kirby-Docken, and H. W. Schnopper, J. Phys. B **9**, L25 (1976); J. R. Mowat, Nucl. Instrum. Methods Phys. Res. Sect. B **10/11**, 108 (1985).

[19] W. Heitler, *The Quantum Theory of Radiation* (Clarendon, Oxford, 1954), p. 242; A. Yamadera, K. Ishii, K. Sera, M. Sebata, and S. Morita, Phys. Rev. A **23**, 24 (1981); H. W. Schnopper and J. P. Delvaille, in *Atomic Collisions in Solids,* edited by S. Datz, B. R. Appleton, and C. D. Moak (Plenum, New York, 1975), p. 488, Eqs. 22 and 23.

[20] F. Biggs, L. B. Mendelsohn, and J. B. Mann, At. Data Nucl. Data Tables **16**, 201 (1975).

[21] D. K. Olsen, K. A. Erb, C. M. Jones, W. T. Milner, D. C. Weisser, and N. F. Ziegler, Nucl. Instrum. Methods Phys. Res. Sect. A **254**, 1 (1987).

[22] J. F. Ziegler, *The Stopping and Ranges of Ions in Matter* (Pergamon, New York, 1980), Vols. 3 and 5.

[23] T. C. Awes, STOPX, a computer program using formulas from Ref. [22] to calculate stopping powers which are numerically integrated for energy losses.

[24] A. B. Wittkower and H. D. Betz, At. Data Tables **5**, 113 (1973), p. 131; F. W. Martin, Phys. Rev. Lett. **22**, 8 (1969).

[25] *Handbook of Spectroscopy,* edited by J. W. Robinson (CRC, Boca Raton, FL, 1979), Vol. I, Table 3.

[26] L. R. Andersson and J. Burgdörfer, in *Physics of Electronic and Atomic Collisions, XVIIIth International Conference,* edited by T. Andersen, B. Fastrup, F. Folkmann, H. Knudsen, and N. Andersen, AIP Conf. Proc. No. 295 (AIP, New York, 1993).

[27] J. H. Scofield, Center for X-Ray Optics X-Ray Data Booklet LBL-Pub-490-Rev, edited by D. Vaughan, 1986 (unpublished); calculated using the relativistic Hartree-Fock code of I. P. Grant *et al.,* Comput. Phys. Commun. **21**, 207 (1980).

[28] L. C. Tribedi, V. Nanal, M. R. Press, M. B. Kurup, K. G. Prasad, and P. N. Tandon, Phys. Rev. A **49**, 374 (1994).